STRUCTURAL RESPONSIVENESS OF FILAMENTOUS BACTERIOPHAGE PF1: COMPARISON OF VIRION STRUCTURE IN FIBERS AND SOLUTION

The Effect of Temperature and Ionic Strength

LEON SPECTHRIE, JEAN GREENBERG, MARC J. GLUCKSMAN, JANET DIAZ, and LEE MAKOWSKI
Department of Biochemistry and Molecular Biophysics, Columbia University, New York, New York, 10032

ABSTRACT X-ray diffraction from fibers and magnetically oriented solutions has been used to study the effect of changes in environment on the helical symmetry and radial structure of the Pf1 virus particle. Detailed analysis of equatorial scattering to a spacing of 8–10 Å was used to identify small radial motions of structural elements in the virus particle. *R*-factor ratios were used to determine the statistical significance of observed changes. Comparison of the structure of virus particles in fibers with those in solution indicated that the helical symmetry of the virions remains unchanged during fiber formation. In most fibers the virions appear to be slightly distorted by the tight packing of virus particles. This distortion results in an apparent increase in the radius of the virus particle of ~0.6 Å. A change in the radius of the DNA is also observed. Increase in the concentration of solvent molecules during fiber formation results in penetration of the virus interior by some solvent components. NaCl is also able to enter the virus interior. The change in the helical symmetry of the virions at ~8°C appears to be the same whether observed by diffraction from fibers or from solutions. Only subtle changes in radial structure are associated with the temperature transition.

INTRODUCTION

The Pf1 virus particle consists of a helical assembly of small, hydrophobic protein subunits surrounding an elongated, single-stranded, circular DNA genome making up a flexible, cylindrical particle ~60 Å in diameter and 19,000-Å long (for a review, see Makowski, 1984). There are ~7,200 copies of the major coat protein arranged in a simple helix with ~5.4 subunits per turn and an axial translation of ~2.7 Å per subunit. There is one nucleotide per coat protein and a few copies of one or more additional structural proteins at each end of the virion. The DNA is extended along the length of the virion with most of its mass being confined to within 10 Å of the long axis of the phage particle (Marvin and Wachtel, 1975, 1976; Makowski et al., 1980). The DNA is surrounded by two layers of alpha helices (Makowski et al., 1980). The inner layer, centered at a radius of ~15 Å, contains the COOH-terminal portion of each coat protein; the outer layer, centered at ~25-Å radius, contains the NH_2-terminal half of each protein. The alpha helices in the inner layer are tilted by ~6° from the virion axis and those in the outer layer are tilted by ~25° from the axis. The interface between these two layers of alpha helices consists almost entirely of hydrophobic amino acid residues (Makowski, 1984). Pf1 virions in oriented fibers prepared above 8°C have a helical symmetry with 5.40 subunits per turn; those in fibers prepared below 8°C have 5.46 subunits per turn (Wachtel et al., 1976; Nave et al., 1979). On decreasing temperature, the slight decrease in angular interval between subunits from 66.7° to 65.9° is accompanied by an increase in the axial displacement between subunits from 2.85 to 3.06 Å. Density, circular dichroism, and microcalorimetric measurements (Hinz et al., 1980) and Raman spectroscopy (Thomas et al., 1983) all indicate that structural changes occur in the Pf1 virion between 5° and 25°C. Dynamic light scattering (Sasaki and Fujime, 1986) indicates that the Pf1 virion is more flexible above the temperature transition than below. These measurements indicate that the transition occurs at 8°C at pH 8.1 and at 11°C at pH 6.9. Measurement of the high field magnetic birefringence of Pf1 in solution (Torbet and Maret, 1981) indicates that the alpha helical segments are more nearly parallel to the virion axis in the low temperature form than in the high temperature form. Comparison (Makowski, 1984) of the electron density maps of Pf1 in fibers prepared at room temperature (Makowski et al., 1980) with those from Pf1 in fibers prepared below 8°C (Nave et al., 1981) indicates that the NH_2-terminal alpha helices on

Address correspondence to Dr. Lee Makowski, Department of Biochemistry and Molecular Biophysics, Columbia University, 630 W. 168th St., NY, NY 10032.

the outer surface of the virion are tilted ~4° closer to the axial direction in the low temperature form than in the high temperature form.

The exact helical symmetry of Pf1 is sensitive to environment. Binding of heavy atoms to Pf1 alters the helical symmetry (Nave et al., 1981; Marvin et al., 1981). In those cases reported, binding of the heavy atoms switches the symmetry towards the low temperature form even at room temperature. Reported symmetries range from 5.39 to 5.46 subunits per turn. This is a much larger range than observed in heavy atom derivatives of the rigid helical virus, tobacco mosaic virus (49.019–49.024 subunits in three turns [Stubbs and Makowski, 1982]).

The Pf1 virion also appears to be structurally responsive to changes in salt concentration. Changes in the Raman spectra of Pf1 have been reported (Thomas et al., 1983) over the concentration range of 0–150 mM NaCl. These changes have been interpreted as indicating changes in the environment of some of the carbonyls and methylene groups in the coat protein with little if any change in the secondary structure. A contribution from the DNA to the spectral changes cannot be ruled out (Thomas et al., 1983).

Filamentous bacteriophage Pf1 can be made to form very highly oriented fibers capable of yielding high resolution structural information (Torbet and Maret, 1979; Nave et al., 1979). However, the environment of a phage particle in a fiber is very different from that in solution. Because of the responsiveness of the Pf1 virion to changes in its environment, it is possible that its structure in solution may be different from that in a fiber. Data from these highly oriented fibers are currently being analyzed with the goal of obtaining a high resolution structural image of the virion. Consequently it is important to characterize the relationship between the structure of the virion in a fiber to its structure in solution. The use of x-ray diffraction from magnetically oriented solutions (Glucksman et al., 1986) allows the collection of diffraction data to 7–10 Å resolution from relatively dilute (18–60 mg/ml) solutions of phage particles. These can be compared with data from partially dried, highly oriented fibers to determine if any gross movement of structural elements occurs during the formation of fibers.

The use of diffraction from magnetically oriented solutions has several advantages over the use of diffraction from fibers even though the potential resolution of the method appears to be limited. Most important of these advantages is the ability to very accurately control the environment of the phage particles. During the formation of a fiber the ionic strength of the sample may increase 100-fold or more and the final concentrations of molecules in the solvent will be uncertain. This makes oriented solutions much more desirable specimens than fibers for the study of the structural effects of temperature and ionic strength. Although limited resolution precludes their use for characterization of small structural changes such as side chain bond rotations, small gross movements of structural elements such as alpha helices can be observed. In this study we have concentrated on the analysis of equatorial scattering, which provides information about the average radial electron density distribution in the phage particles. This allows characterization of radial movements of structural elements in the virion particle.

To a resolution of 7 Å, the amplitudes along the equator of a diffraction pattern from Pf1 correspond to the Fourier transform of the axially and cylindrically averaged electron density distribution. In the notation of Klug et al. (1958), to 7-Å spacing, the amplitudes on the equator have only one term, $G_{0,0}(R)$, which is the zero-order Fourier–Bessel transform,

$$G_{0,0}(R) = \int_0^\infty g_{0,0}(r)\, J_0(2\pi rR)2\pi r\mathrm{d}r, \qquad (1)$$

of $g_{0,0}(r)$, the axially and cylindrically averaged electron density:

$$g_{0,0}(r) = (1/2\pi) \int_0^c \int_0^{2\pi} \rho(r, \phi, z)\mathrm{d}\phi\mathrm{d}z. \qquad (2)$$

In this paper $g_{0,0}(r)$ will be referred to as the radial density profile. Beyond 7-Å spacing noncylindrically symmetric components of the equatorial scattering become important. These will not be considered here.

Although the radial transform can be obtained to only 7–10 Å spacing in diffraction from these samples, small changes in the positions of nodes in the transforms or in the relative peak heights can be used to map very small changes in the radial positions of structural features. A critical step in the data analysis is a statistical analysis of small differences between data sets to determine if the differences are significant. This is particularly important for the comparison of data from fibers and from oriented solutions. The equatorial data from fibers are sampled on a hexagonal grid due to the hexagonal close packing of virions in the fibers. The equatorial data from oriented solutions are essentially continuous scattering corresponding to the Fourier transform of a single particle. Any interference effects in this scattering are at very low angles not observed in the experiments described here. To compare these two kinds of data we have built models for the radial density profiles and refined the parameters of these models against both the fiber and solution data. Because of the structural information available for PF1 this approach provides a means for putting the data on an absolute scale. Quantitative use of R-factor ratios (Hamilton, 1965) then provides a means for discriminating between data sets corresponding to the same structures and data sets corresponding to different structures.

METHODS

Preparation of Specimens

Oriented fibers of Pf1 virions were prepared as described previously (Makowski et al., 1980) or in the bore of a 5.8-Tesla superconducting magnet using methods essentially as described in Nave et al. (1981). Pf1

solutions at 30–50 mg/ml initially in 10 mM Tris-HCl buffer at pH 8 were dried over a period of days against saturated salt solutions to relative humidity of ~92%. The final proportion of solvent in the fibers was in the range of 25–35% by weight (65–75% virions) as determined by measurement of lattice constants and axial repeat distances. The surface of selected fibers was coated with finely ground NaCl, which was absorbed into the fibers over a period of hours.

Oriented solutions of Pf1 were obtained by placing dilute virus solutions in 0.7-mm thin-walled quartz capillaries between the poles of a small permanent magnet generating a field of ~1.6 Tesla in a volume of 1 mm^3 (Glucksman et al., 1986). Virus concentration was usually 19.5 mg/ml in 10 mM Tris-HCl buffer at pH 8. When NaCl was added, it was to a final concentration of 150 or 300 mM. Diffraction patterns from these specimens were taken while the specimen was in the magnetic field. Orientation of these specimens was not stable in the presence of x-rays when they were removed from the field.

X-ray Diffraction

X-ray diffraction patterns were obtained using Cuk_α radiation from a rotating anode x-ray source (Rigaku USA Inc., Danvers, MA) or using 1.54-Å synchrotron radiation at the CHESS facility at Cornell. X-rays from the rotating anode source were focused with a camera using two bent, totally reflecting mirrors. Particular care was taken to maintain specimen and film positions fixed to maximize accuracy of specimen-to-film distance measurements. Consistency of data taken at Cornell and Columbia on identical specimens indicated that the specimen-to-film distance was determined to better than 0.5%. Diffraction patterns were recorded on Kodirex film (Eastman Kodak Co., Rochester, NY) and densitometered on a 50-or 100-μm raster using an Optronics P1000 rotating drum microdensitometer. Densitometer traces of the equatorial scattering were obtained by averaging over 2° to 4° arcs.

Equatorial diffraction from fibers consists of a series of sharp reflections indexing on a hexagonal lattice. Background was subtracted by drawing a smooth line connecting the background on either side of each Bragg reflection. Intensities were estimated by manual integration of the area of the peak. Geometric corrections on the measured intensities, I, included multiplication by a factor of R (distance from the origin of reciprocal space) for disorientation correction, a factor of R for Lorentz correction, and an additional factor for reflection multiplicity,

$$|F| = (IR^2M)^{1/2} \tag{3}$$

where, for reflection (h,k),

$$M = \begin{cases} 1.0 \text{ if } h = k,\ h = 0, \text{ or } k = 0 \\ 0.5 \text{ otherwise.} \end{cases} \tag{4}$$

The amplitudes of reflections on the equator will be real since they correspond to the Fourier transform of a cylindrically symmetric, two-dimensional object. Their phases have been obtained previously (Marvin and Wachtel, 1976; Makowski et al., 1980) and the same phases are used throughout. Under no conditions studied was there an indication that the phase of a reflection changed due to structural change of the virion in the fibers.

Equatorial diffraction from magnetically oriented solutions is continuous diffraction with no sampling apparent. In most cases, the distribution of orientations of virions in solutions as judged by arcing of reflections in diffraction patterns did not have a half-width of <4°. Since the amplitudes along the equator are real and the minima in the measured intensities all correspond to points where the phase of the amplitudes is expected to change, the minima were assumed to represent real zeros in the diffracted intensities. A sum of quadratics was fit to the positions of the minima and used as an estimate for the background between minima. For diffraction patterns where the signal-to-noise ratio was particularly low, the data were smoothed by convolution with a triangle function (linear smoothing) before background subtraction. Geometric corrections included only the disorientation correction as described above. For diffraction from oriented solutions there are no Lorentz or multiplicity corrections. Phases were chosen to be as consistent as possible with those from fibers. This indicated that phases changed at each apparent zero of the continuous measured intensities.

Model Building

Quantitative comparisons of diffraction data from fibers and from solutions are particularly difficult when, as in this study, the interest is in small differences in the structure of the diffracting particles in different specimens. Scaling of data sets is important and, lacking additional information, usually ambiguous. The approach taken here is that of model building. Previous work (Makowski et al., 1980) indicated that the radial profile of Pf1 at 7-Å resolution consists of three peaks; one at the center of the particles, corresponding to DNA; one at ~15-Å radius corresponding to the layer of COOH-terminal alpha helices; and one at ~25-Å radius corresponding to the layer of NH_2-terminal alpha helices. This radial density profile is well represented by the sum of three Gaussians. The entire profile can be characterized by nine parameters: the heights, widths, and positions of these three Gaussians. Comparison of calculated with observed intensities indicates that this form of a model can be used to fit accurately all the data sets considered here. The nine parameters used to fit the data are h_i, r_i, and w_i, $(i = 1,3)$ defined as

$$g_{o,o}(r) = \sum_{i=1}^{3} h_i \exp\left[-(r - r_i)^2/2w_i^2\right], \tag{5}$$

where $i = 1$ corresponds to the central peak and $i = 2$ and 3 correspond to the peaks at successively increasing radii. The reference electron density, at zero in this equation, corresponds to the average electron density in the specimen. For solutions this will be essentially identical to solvent electron density, but for fibers, which are <50% solvent, this density will be substantially greater than solvent electron density. The electron density profile corresponding to a model can be put on an absolute scale by equating

$$2\pi c \int_0^\infty g_{o,o}(r)\, r\, dr, \tag{6}$$

where c is the axial rise per subunit, with the total number of electrons in excess of solvent electrons in a subunit (electrons in the subunit minus the number of solvent electrons displaced by the subunit). This number can be calculated from the amino acid sequence, the expected volumes for each amino acid (e.g., from Chothia, 1975) and the specific volume of DNA (Makowski and Caspar, 1978). The total number of electrons in excess of water (using as the electron density of water, 0.334 electrons/$Å^3$) for the Pf1 coat protein is 440.9 and for one average nucleotide is 58.2.

Calculations with the nine-parameter models indicated that in the fibers the average electron density was greater than the electron density expected at ~20-Å radius in the protein coat (see Results). The nine-parameter models only allow for electron density positive relative to the average, Eq. 5. Consequently, although it is possible to choose nine parameters to obtain an adequate fit to the data, it is not clear that the corresponding model is an accurate representation of the electron density profile. An alternative model strategy was formulated in which the model was initially constructed relative to the electron density of water and the electron density profile was then adjusted to reflect the average electron density for the specimen being modeled. This required specific assumptions about solvent penetration into the virus: At the outer surface of the virus the proportion of solvent excluding space was taken to be proportional to the electron density. At radii below that of the outer peak, the model was treated as if there were no solvent penetration. The model parameters thus derived reflect not only the intrinsic virus structure but also solvent penetration.

Final model building calculations used only seven parameters. Two parameters were removed by constraining the total number of electrons in

excess of water to be constant for the two peaks representing the two layers of alpha helices. This was done because refining an unconstrained model against data sets missing data near the central maximum results in a set of equally acceptable electron density profiles differing only in the tilt of a baseline. This ambiguity is described in detail by Earnshaw et al. (1976). Constraining the total number of electrons in excess of solvent in each of these two peaks removes this ambiguity.

RESULTS

Diffraction Data from Fibers and Solutions

Fig. 1 contains a diffraction pattern from a fiber (*a*) and from a magnetically oriented solution (*b*) of Pf1. The diffraction pattern from the fiber was chosen because the degree of disorientation in that fiber was comparable to that in the magnetically oriented solution. Many of the fibers prepared in the 5.8-Tesla field had much better orientation than this pattern (e.g., see Makowski, 1984). The equatorial data from the fibers consist of a series of sharp Bragg reflections present along a horizontal line intersecting the center of this diffraction pattern. These sampled reflections could be measured accurately to 8–10-Å resolution. The equatorial diffraction from the oriented solutions consisted of a series of broad diffraction fringes measurable to ~10-Å spacing. Comparison of the data from fibers with that from solutions indicates that the weak Bragg reflections usually fall near the spacing of nodes in the continuous diffraction amplitudes.

Fig. 2 contains densitometer traces along the equators of a fiber pattern (*a*) and a diffraction pattern from a magnetically oriented solution (*b*). In these drawings the background subtracted from the data is indicated by broken lines. Bragg sampled data from the fiber are readily measured and the backgrounds well determined. Data from the solutions have a lower signal-to-noise ratio and,

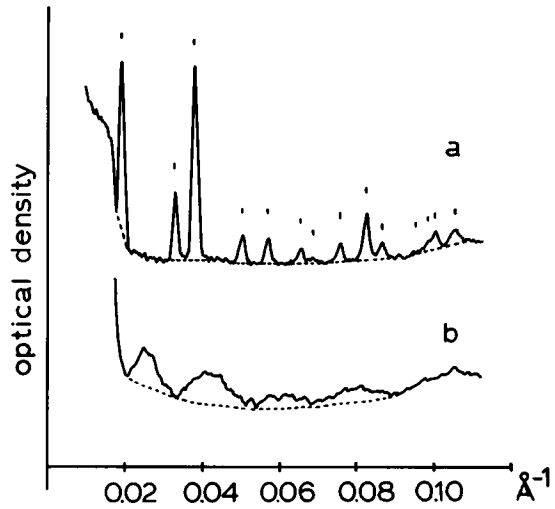

FIGURE 2 Densitometer traces along the equator of a diffraction pattern from (*a*) a fiber and (*b*) an oriented solution of Pf1. The expected positions of Bragg reflections are marked above the trace in *a*. The background subtracted from the raw data is marked as a broken line.

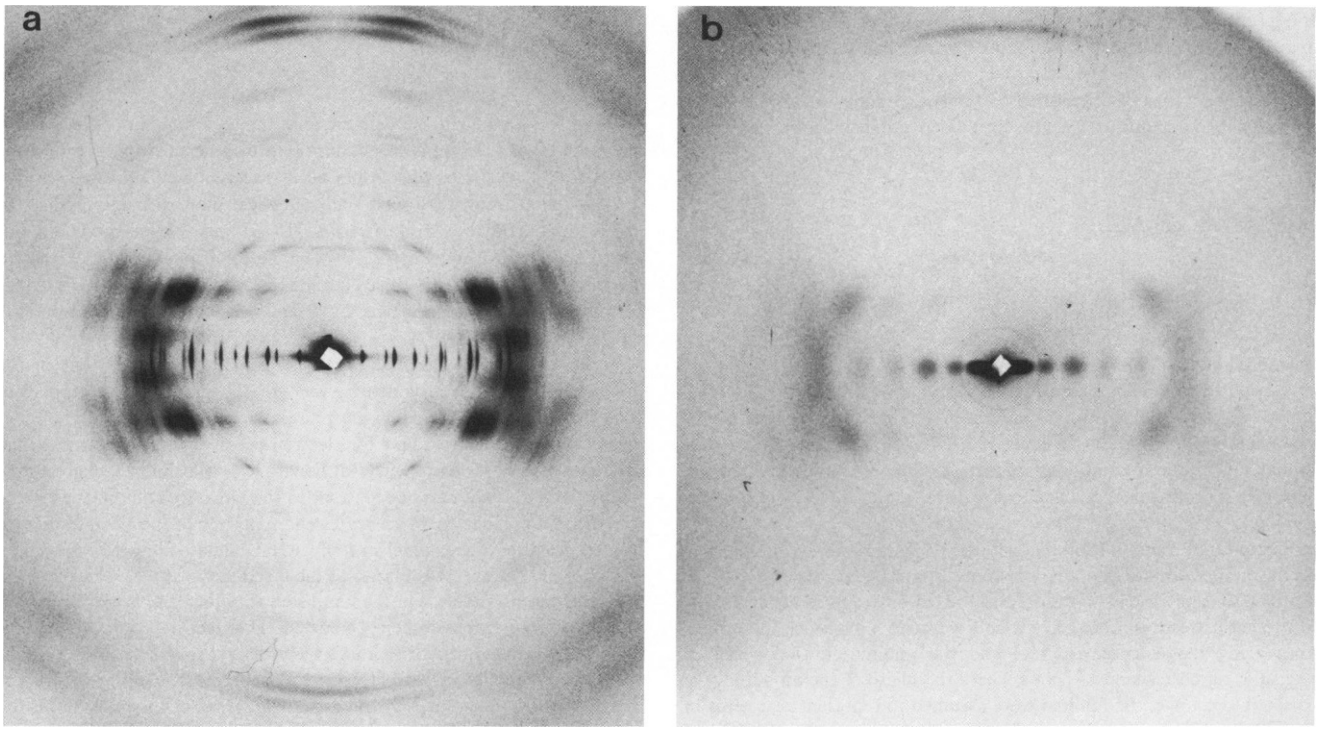

FIGURE 1 X-ray diffraction patterns from (*a*) a fiber of Pf1 and (*b*) an oriented solution of Pf1. In the diffraction pattern from the fiber the equator consists of a series of sharp Bragg reflections corresponding to the two-dimensional hexagonal lattice of closely packed virions in the fiber. In the diffraction pattern from the oriented solution the equator is made up of a series of diffraction fringes representing continuous intensities.

since the background is well determined at only five points, there is more uncertainty in the peak heights.

Symmetry

The helical symmetry of Pf1 under different conditions is more difficult to estimate accurately from diffraction patterns from solutions than from fibers. In both cases, the positions of layer lines were estimated by traces of optical density as a function of angle about the center of the diffraction pattern at constant radius. The subunit axial rise, h, and angular interval, Ω, were then estimated (Moody and Makowski, 1981) from the distance of the third and fifth layer lines from the equator.

Fig. 3 is a plot of typical values of h and Ω for fibers and solutions. The open circles are from fibers, closed circles from solutions, and crosses from fibers to which NaCl has been added. No solution containing salt was oriented well enough to make an accurate determination of symmetry. All specimens with $\Omega < 66.5°$ were prepared at low temperature (<8°C). All specimens with $\Omega > 66.5°$ were prepared above 8°C. No distinction between fibers and solutions is apparent from these measurements. Addition of salt to fibers appears to have the effect of lowering h. This was observed in the same fibers before and after the addition of salt. This change was not expected in view of the close interparticle packing within the fibers that has the effect of preventing (Wachtel et al., 1976) or retarding (Specthrie, L., unpublished observations) the symmetry changes associated with the temperature transition. Once fibers are formed, the symmetry of the virions in the fiber does not change in response to changes in temperature. Change in the symmetry of particles in response to addition of salt may be made possible by the effect of NaCl on interparticle packing. In most cases, some disordering of the two-dimensional hexagonal lattice was observed. The changes in symmetry in response to NaCl addition, although small, appear to represent significant changes in the Pf1 virion structure.

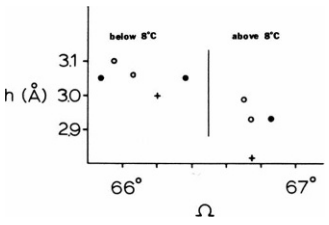

FIGURE 3 Helical symmetry of Pf1 under different environmental conditions. Ω is the angular interval between subunits and h is the axial spacing of subunits. All specimens prepared below 8°C have an $\Omega < 66.5°$ and all specimens prepared above 8°C have an $\Omega > 66.5°$. Open circles correspond to virus in fibers, solid circles correspond to virus in solution. To within the experimental errors involved in the measurements these two populations appear to be identical both at high and low temperatures. The crosses represent virions in fibers to which NaCl has been added. These appear to have a slightly different axial repeat as measured from the same fibers before and after addition of NaCl.

Comparison of Scattering Amplitudes

There are three steps in determining whether or not the environmental changes studied here have a significant effect on the radial structure of Pf1. The first is to determine whether or not there are differences in the data. The second is to interpret any differences in data based on comparisons of radial density profiles. The third is to determine whether or not any observed differences in profiles are statistically significant.

The first step, determining whether there are differences in the data, is difficult when data from solutions and from fibers are being compared. The best method for scaling these data sets is not immediately clear. The method used here was to fit all the data to nine-parameter models and then to scale all data sets based on the calculated continuous amplitudes. For this process, the heights of the diffraction fringes at 0.04, 0.06, and 0.08 $Å^{-1}$ were used. This scaling minimized the apparent differences among data sets.

Data from fibers and solutions are compared in Fig. 4 for specimens prepared above 8°C (a) and for specimens prepared below 8°C (b). In both cases there is a shift in the scattering amplitudes to lower spacings in the fiber data

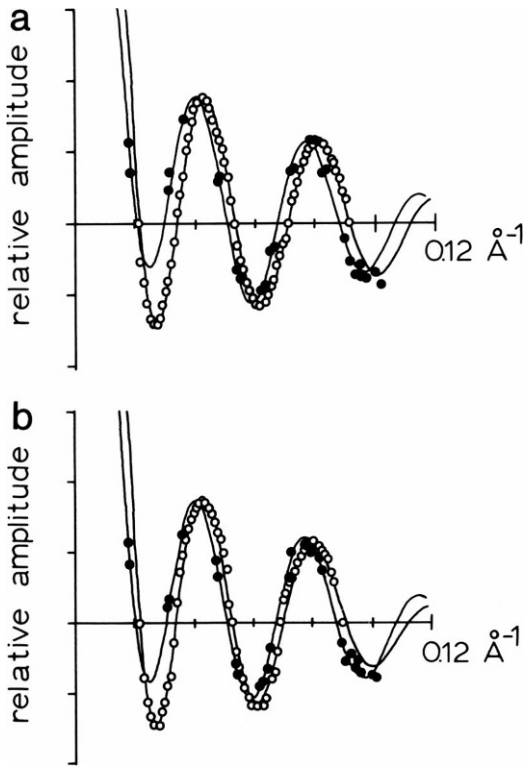

FIGURE 4 Comparison of equatorial amplitudes in diffraction from fibers and from solutions taken using specimens (a) prepared above 8°C and (b) prepared below 8°C. The solid circles correspond to fibers, the open circles to solutions. The solid lines correspond to the amplitudes calculated for the best model to the data. It is clear from these two plots that the equatorial amplitudes from fibers are significantly shifted relative to those from solutions.

compared with the solution data. These differences were found uniformly for all data sets measured.

Fig. 5 is a comparison of data from specimens prepared above and below 8°C. Data from solutions are shown in Fig. 5 *a* and data from solutions with 300 mM NaCl added are shown in Fig. 5 *b*. Data from fibers are shown in Fig. 5 *c* and from fibers to which NaCl has been added in Fig. 5 *d*. Little or no systematic differences are seen in the equatorial transforms of solutions above and below 8°C in the absence of NaCl. However, in 300 mM NaCl small apparent differences in the transforms can be seen. Similar behavior is seen in fibers. In the absence of salt there is no apparent difference between the data from fibers prepared above and below 8°C. With the addition of NaCl, however, systematic differences are observed. Apparently NaCl may modulate the effect of the temperature transition on the radial structure of Pf1.

Fig. 6 compares data from specimens in the presence and absence of salt. In warm solutions, the addition of 300 mM salt appears to have only a small effect as seen in Fig. 6 *a*. Some changes in the relative heights of diffraction fringes are observed, but they are small. In cold solutions (Fig. 6 *b*), the same behavior is observed but the effect is larger. Fig. 6 *c* includes data from fibers prepared at room temperature before and after the addition of NaCl. Significant differences are observed. One problem in comparing data from fibers before and after the addition of salt is that the salt appears to disorder the hexagonal lattice in the fiber. In the presence of salt, the reflections were, on average, broader and the limiting resolution lower. Plots of the ratio of structure factors from specimens with identical lattice constants in the presence and absence of salt suggested that the differences cannot be accounted for solely by a disordering of the lattice. Similar behavior was observed in fibers prepared in the cold (Fig. 6 *d*).

Plots comparing data from identically prepared specimens were also examined to determine the reproducibility of the data. Variations in data from solutions were small and were never more than the diameter of a single data point as drawn in Figs. 4–6. When small differences were observed they were in the relative heights of diffraction fringes and indicative of small errors in the background subtraction. No significant shifts of node or peak positions were observed. Data from fibers were of comparable quality with somewhat higher variation in the highest resolution reflections. Comparisons among fibers were more difficult because of small variations in the lattice constant over the range 60–63 Å. Nevertheless, the varia-

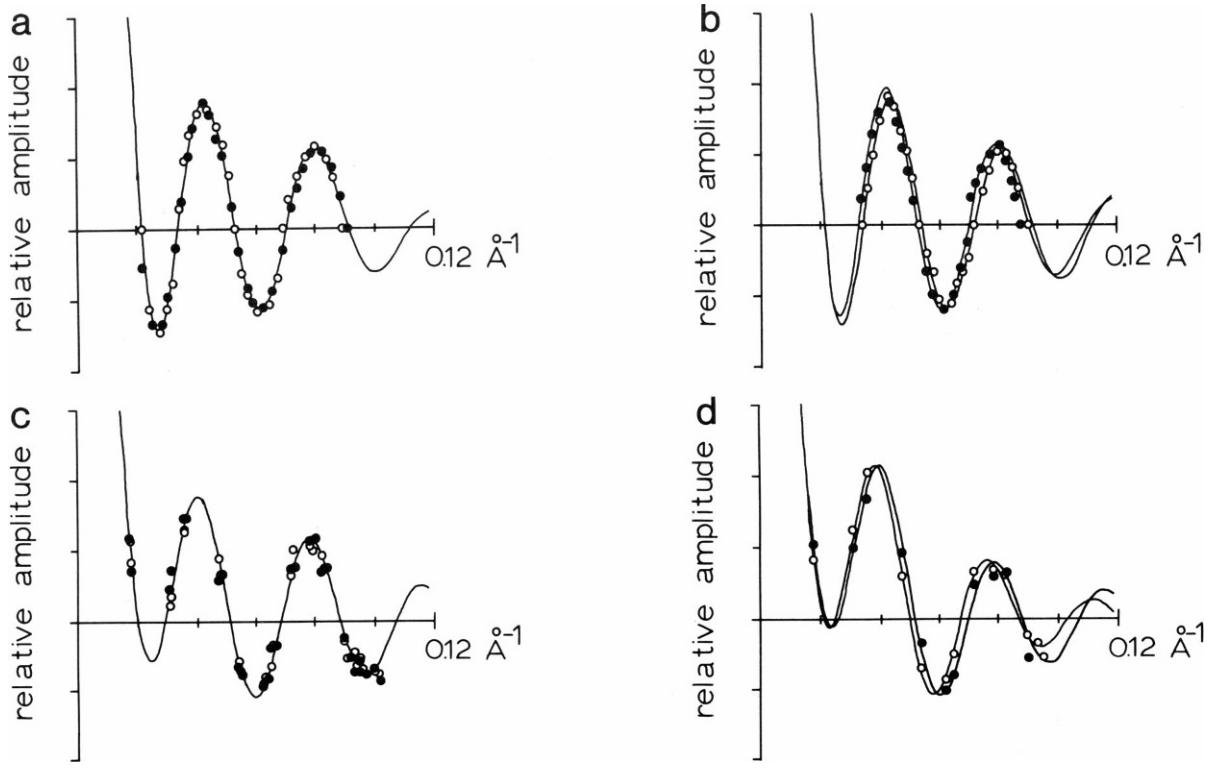

FIGURE 5 Comparison of equatorial amplitudes in diffraction from specimens prepared above and below 8°C. Plotted are amplitudes from specimens in (*a*) solutions, (*b*) solutions with 300 mM NaCl added, (*c*) fibers, and (*d*) fibers to which NaCl was added. Data for specimens at temperatures above the transition temperature are given as solid circles, those below the transition temperature are shown as open circles. In the absence of NaCl essentially no differences in the equatorial transform were detected in the comparison of specimens prepared above and below the transition temperature. In the presence of NaCl small but significant differences were observed. In the case of diffraction from solutions only representative data points were plotted to allow direct comparison of similar data sets.

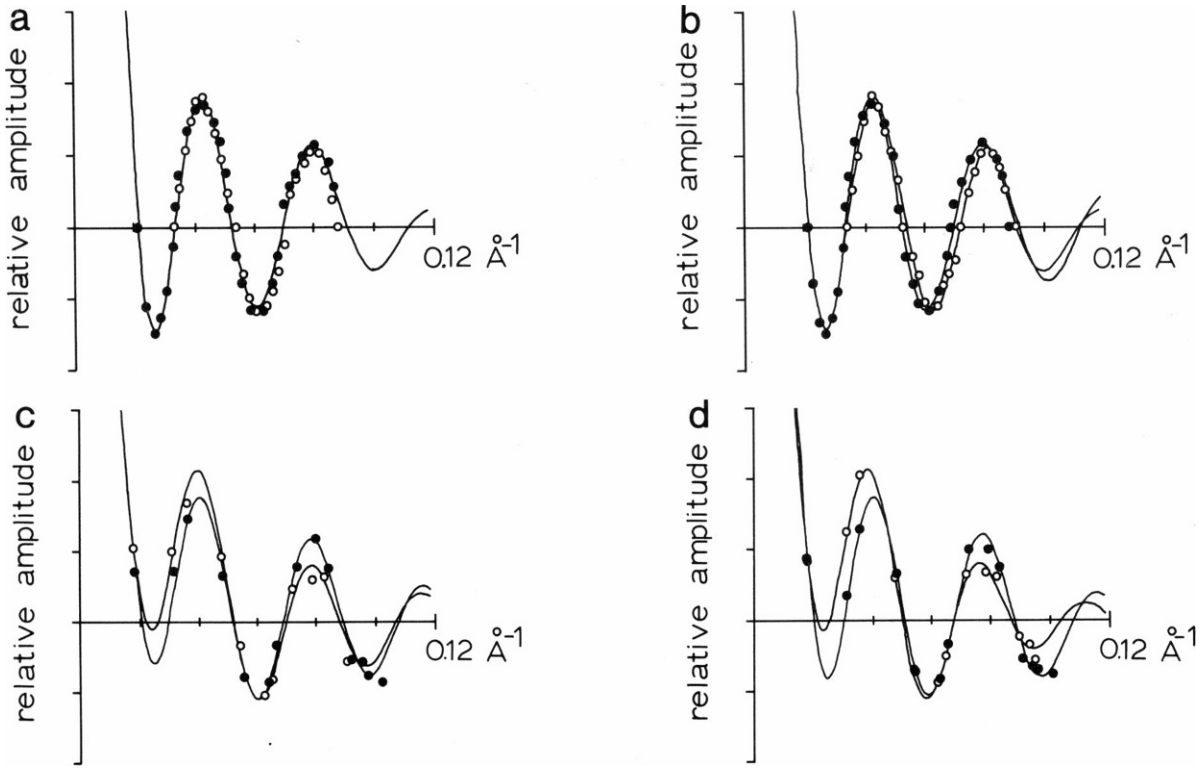

FIGURE 6 Comparison of equatorial amplitudes in diffraction from specimens in the presence and absence of NaCl. Plotted are amplitudes from (*a*) solutions above the transition temperature, (*b*) solutions below the transition temperature, (*c*) fibers above the transition temperature, and (*d*) fibers below the transition temperature. Solid circles correspond to specimens in the absence of NaCl, open circles to specimens to which NaCl has been added. Small differences are seen for diffraction from solutions and somewhat larger differences are seen in the case of fibers.

bility observed indicated that the differences noted above represent significant differences in the scattering amplitudes from differently prepared specimens.

Nine-Parameter Models

All data sets were fitted to nine-parameter models consisting of three Gaussians of variable heights, widths, and radii. From these parameters the total number of electrons, e_j (on an arbitrary scale), associated with each Gaussian was calculated. A partial list of these is given in Table I. Comparison of the e_j for several different specimens indicates that these parameters cannot characterize similar structures. For instance, the ratio of total scattering density in the peak near 25-Å radius (peak 3) to that of the peak near 15-Å radius (peak 2) is >3 for all fibers and <2 for all solutions. This observation can be accounted for by variations of the average electron density of different specimens.

TABLE I
NINE-PARAMETER MODELS

	Fibers				Solutions	
T	Warm	Cold	Warm	Cold	Warm	Cold
Na	–	–	+	+	–	–
e_1	30.5	30.8	39.0	41.3	28.5	24.1
e_2	34.3	33.3	24.2	18.2	49.0	57.5
e_3	94.2	95.0	95.8	99.6	81.5	77.4

Total scattering density, e_j, associated with each of the three Gaussian peaks used in the nine-parameter models (on an arbitrary scale). The very large differences between the e_j for fibers and for solutions is due to the difference in average electron density in the two types of specimens. These numbers were used to estimate the average electron density in the two types of specimens as described in the text.

The relative number of electrons in excess of average in each peak in the nine-parameter models can be used to derive the average electron density in each specimen given some assumptions about the coat protein structure. The number of electrons in excess of average associated with each peak is equal to $(N_j - \rho_{ave}v_j)$, where N_j is the total number of electrons and v_j is the total volume displaced. The ratio,

$$R_j = (N_j - \rho_{ave}v_j)/(n_3 - \rho_{ave}v_3) = e_j/e_3 \qquad (7)$$

can be determined from the e_j in Table I. The average electron density can be derived from these using the relationship

$$\rho_{ave} = (R_jN_3 - N_j)/(R_jv_3 - v_j) \qquad (8)$$

for $j = 1, 2$. To use this relationship, some assumption about the distribution of protein and DNA among the peaks must be made, that is, N_j and v_j must be determined. These assumptions can be evaluated based on the self

consistency of the derived electron densities. The distribution of protein and DNA giving the best self consistent average electron densities placed residues 1–27 as constituents of the outer peak and 28–46 within the inner peak. This is consistent with the 7-Å resolution three-dimensional electron density maps (Makowski et al., 1980; Nave et al., 1981) and the dissection of the radial profile in 10 mM Tris-HCl into two peaks. The average electron density derived in this manner for fibers is 0.375 e/Å^3 and for fibers with added salt, 0.387 e/Å^3.

The average electron densities expected for fibers can be estimated from the initial concentration of virus and Tris-HCl in the starting material, the lattice constant of the fiber, and the electron densities of Tris-HCl solutions and the virus. From lattice constant measurements, the average concentration of Tris in the fibers is in the range of 0.8 M, giving the solvent an electron density of ~0.344 e/Å^3. The average electron density of the virus particle is ~0.413 e/Å^3. This results in an average electron density for the fibers of ~0.38 e/Å^3, very close to that calculated from the results of the nine-parameter models. Using Eq. 8, the concentration of NaCl in the fibers to which it was added can be calculated to be in the range of 2.5–3.0 M. This is a reasonable number given the method by which the NaCl was added and indicates that the NaCl concentration in those fibers was about 10 times that in the high salt solutions described here.

The very high average electron densities calculated indicate a problem with the nine-parameter models: There may be some portions of the radial density profile with average density lower than the baseline. This cannot be modeled using the formalism adapted here. Consequently, the nine-parameter models were used to estimate the baseline electron density but they were not used to define the structural parameters of the virus particles under different conditions.

Seven-Parameter Models

A set of seven-parameter models were refined against all data sets. In these models the radial profile was constructed in two steps: The profile was calculated from the model parameters relative to the electron density of water (0.334 e/Å^3) with the total number of electrons in excess of solvent held fixed for the two electron density peaks corresponding to protein. The profile was then computed for the baseline electron density determined from the nine-parameter models in a way that allowed for some penetration of solvent into the outer portion of the virus structure but not into the interior. In these models any penetration of solvent into the virus interior is reflected in changes in the total number of electrons in excess of solvent associated with the central peak. Consequently, differences in model parameters may reflect either structural differences in the virus under different conditions or different degrees of solvent penetration. Separating these two effects in the model refinement would have required more parameters than could have been reliably defined by the available data. The radial density profiles resulting from the seven-parameter models were put on an absolute scale using the total number of electrons in excess of solvent and the subunit axial repeat.

Table II is a list of the derived model parameters for 12 of the best diffraction patterns collected. Included in the list is the number of electrons in excess of solvent calculated for the first peak. Examination of these parameters suggests that there are significant differences among the structures under different solvent conditions. However, discrimination among very similar models requires careful statistical treatment. For this we used Hamilton's significance tests. The normalized R-factor was calculated for each model against every data set (using amplitudes, not intensities, since there was no doubt in phase assignment). When two models have relatively low R-factors for the same data set, it may be impossible to distinguish between the two models based on the data. The R-factor for each of the 12 models listed in Table II was calculated against all 12 data sets. These R-factors are listed in Table III. R-factors in semibold italics indicate models that are not significantly worse than the best model found for that particular data set at the 25% level of significance. Those in boldface type are not significantly worse at the 50% level of significance. That is, if we rejected these models for a particular specimen we would be wrong at least 25% (50%) of the time. All remaining R-factors represent models that are significantly worse than the best possible model for a given data set (if we chose these models for the data we would be choosing an inferior model more than 75% of the time). Table III includes four pairs of specimens that were identically prepared. In most cases the models for identically prepared specimens could not be distinguished as significantly different. Examination of the R-factors in Table III for specimens 1–4 indicate that there is significant variability in the structure of identically prepared fibers. Results for specimens 7–10 indicate no such variability in identically prepared solutions. The R-factors for specimens 1–4 and 7–10 indicate that there is no consistent, significant difference in the radial profiles of virions at temperatures above and below the temperature transition in either fibers or solutions.

Comparison of the Radial Profiles of Virions in Fibers and in Solution

The radial density profiles of virions in fibers and in solution are compared in Fig. 7 at high temperature (Fig. 7 *a*) and low temperature (Fig. 7 *b*). At least two differences appear to be distinguishable between the structure in fibers and solution: In the fibers the two protein peaks appear to be at a radius ~0.6 Å larger than in virions in solution, and the radius and total volume of the central DNA peak is also larger in virions in fibers. These radial differences represent a statistically significant structural

TABLE II
MODEL PARAMETERS

	Fibers						Solutions					
T	Cold	Cold	Warm	Warm	Cold	Warm	Cold	Cold	Warm	Warm	Cold	Warm
Na	−	−	−	−	+	+	−	−	−	−	+	+
Data set	1	2	3	4	5	6	7	8	9	10	11	12
r_1	4.0	4.0	4.1	3.9	4.2	5.0	2.1	2.1	2.1	2.2	2.6	2.5
h_1	1.84	1.83	1.79	1.89	1.89	1.82	2.16	2.16	2.16	2.12	2.06	2.18
w_1	4.4	4.5	4.6	4.6	4.6	4.1	5.0	5.0	5.0	5.0	4.9	4.9
e_1	89.8	91.8	93.8	95.7	101.2	97.6	86.9	85.5	86.9	86.9	88.8	92.1
r_2	15.5	15.8	15.8	15.7	15.7	16.1	14.5	14.7	14.3	14.5	14.8	14.4
w_2	3.7	3.7	3.8	4.0	4.3	3.8	4.0	4.0	4.0	4.2	4.4	4.3
r_3	25.9	26.3	26.4	26.2	26.3	25.8	25.9	25.9	25.7	25.8	25.6	25.9
w_3	2.5	2.4	2.6	2.3	2.7	2.8	2.6	2.5	2.2	2.2	2.1	2.4

Model parameters derived for the seven-parameter models. The radius, r_j, and width, w_j, of each Gaussian making up the model is given (in angstroms). The height, h_j, and total number of electrons in excess of the electron density of water (0.334 e/Å^3), e_j, is given for the central peak, peak No. 1, on an absolute scale. The total number of electrons in excess of the electron density of peaks 2 and 3 were constrained to be 177.3 and 263.6 as described in the text. Data are given for four pairs of specimens prepared and studied under identical conditions to indicate reproducibility of results.

change that appears to take place during formation of most but not all fibers. The radial shift of the protein peaks is at the borderline of the sensitivity of the method. However, it is reproducible and consistent as documented in Table II and includes both protein peaks. The data suggest that a very small increase in virion radius occurs on formation of most fibers. The statistical significance of these radial changes can be isolated from that of the central peak by constructing models for fibers using the outer peaks from models for virions in solution and varying only the inner peak. This type of calculation indicates that in most fibers the radial motion is significant but in a few it is not. The variability in fiber specimens appears to be intrinsic to the structure in fibers and is not correlated to lattice constant. Changes in the central peak appear to be due in part to increased presence of solvent ions within the virion as indicated by the change in e_1 in Table II. The change in radius of the DNA peak appears to be due to a change in the DNA conformation of radius rather than to increased presence of solvent ions since the increase in e_1 represents a small percentage of the total e_1. Caution should be taken in overinterpreting these changes, however, because at <4–5-Å radius the density profile is poorly determined by 8–10-Å resolution data.

TABLE III
R-FACTOR TABLE

	Fibers						Solutions					
T	Cold	Cold	Warm	Warm	Cold	Warm	Cold	Cold	Warm	Warm	Cold	Warm
Na	−	−	−	−	+	+	−	−	−	−	+	+
Data set	1	2	3	4	5	6	7	8	9	10	11	12
1	**0.119**	***0.195***	0.224	***0.173***	0.291	0.389	0.244	**0.100**	0.186	0.231	0.200	**0.176**
2	0.204	**0.134**	***0.140***	***0.168***	0.287	0.471	0.233	***0.143***	0.271	0.263	0.312	***0.193***
3	0.216	**0.172**	**0.086**	0.208	0.260	0.450	0.263	0.197	0.324	0.304	0.361	***0.225***
4	**0.168**	**0.182**	0.188	**0.118**	0.273	0.392	***0.183***	**0.110**	0.213	0.189	0.232	**0.128**
5	0.219	0.327	0.245	0.277	**0.109**	0.310	0.236	0.217	0.316	0.259	0.303	**0.188**
6	0.320	0.394	0.406	0.382	0.282	**0.141**	0.392	0.272	0.349	0.382	0.234	0.283
7	0.280	0.374	0.317	0.302	0.261	0.415	**0.130**	**0.095**	0.144	***0.121***	0.235	**0.148**
8	0.230	0.324	0.291	0.240	0.268	0.414	**0.135**	**0.085**	0.135	**0.111**	0.215	**0.149**
9	0.269	0.374	0.371	0.272	0.349	0.421	**0.180**	***0.149***	**0.066**	**0.105**	***0.163***	**0.176**
10	0.245	0.344	0.346	0.228	0.329	0.410	**0.163**	***0.130***	**0.087**	**0.079**	***0.147***	**0.149**
11	0.337	0.439	0.476	0.329	0.439	0.439	0.248	0.223	0.172	0.160	**0.084**	***0.225***
12	0.282	0.382	0.332	0.279	0.225	0.348	**0.165**	**0.127**	0.140	0.136	0.187	**0.118**

R-factor table. Each column in this table corresponds to a particular data set. Each row to a particular model. The entries in the table are normalized R-factors (Hamilton, 1965) for each model against all data sets. The jth model represents the least-squares sense best model found for the jth data set. Alternate models with R-factors only slightly greater than the best model may not be statistically inferior to the best model found. The distinction between models that can be rejected and those that cannot be rejected is made based on Hamilton's (1965) significance test. Those R-factors that are in semibold italics represent models for a particular data set that cannot be rejected at the 25% level of significance. That is, if we were to reject them as inferior, we would be making an error at least 25% of the time. Those R-factors in boldface type indicate models that cannot be rejected at the 50% level of significance. The remaining R-factors represent models for data sets that are expected to be inferior at least 75% of the time.

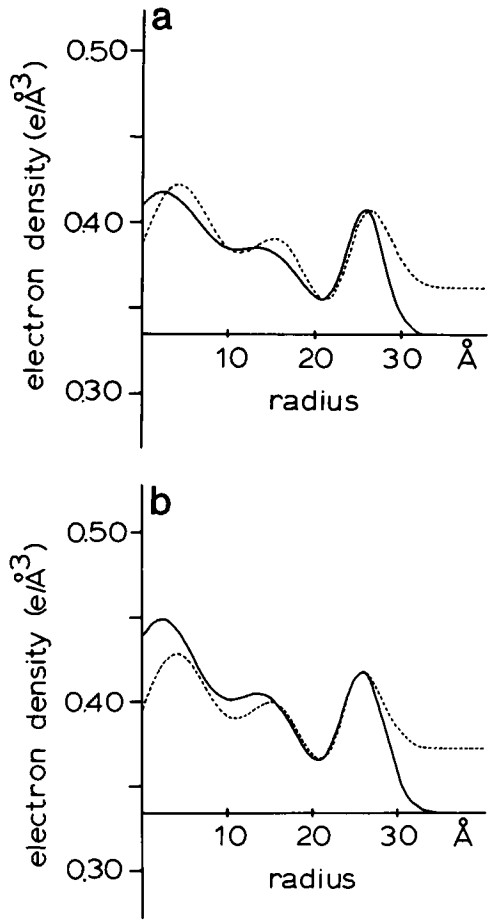

FIGURE 7 Comparison of radial density profiles for virions in fibers and solutions prepared (*a*) above the transition temperature and (*b*) below the transition temperature. Solid lines correspond to virions in solution, broken lines to virions in fibers. There is a variable apparent increase in the radius of the virion by up to 0.7 Å in profiles from fibers compared with profiles from solutions. This includes both density peaks corresponding to layers of alpha helices. A larger increase in the radius of the central peak corresponding to the DNA is uniformly observed. All of the profiles corresponding to virions in fibers in Figs. 7–9 have been rescaled to set the contrast between the top of the peak at ~26-Å radius and the minima at ~21-Å radius to the same value. This has been done for ease in the comparison of the profiles. Since the average electron density of these specimens has been only approximately determined, this rescaling may represent an improvement in the estimate of baseline density. Comparisons made directly from profiles on the absolute scale defined by the seven-parameter models result in the same conclusions as outlined here. This rescaling was not done for profiles for virions in solution since the baseline electron density is not in question.

Effect of Temperature

Comparison of radial density profiles at temperatures above and below 8°C are shown in Fig. 8. Fig. 8 *a* compares density profiles in solution in the absence of added NaCl, and Fig. 8 *b* in the presence of 300 mM NaCl. In both cases the only apparent differences are in the heights and widths of the outer peaks. Examination of Table II indicates that these changes are consistent and reproducible. However, these differences in outer peak widths do not appear to be significant as judged from the *R*-factor ratios in Table III. If there are any radial structural changes associated with the temperature transition in solution they appear to be confined largely to the outer layer of alpha helical segments.

Comparison of density profiles for virions in fibers prepared above and below 8°C are shown in Fig. 8 *c* for fibers in the absence of NaCl and in 8 *d* for fibers to which NaCl has been added. Although there appears to be some radial differences in the profiles in Fig. 8 *c*, the *R*-factor ratios in Table III indicate that these are not statistically significant. The parameters listed in Table II indicate that these radial changes are not reproducible. In the presence of NaCl there appears to be significant structural changes. These appear to involve small changes in all aspects of the radial profile. This is the only comparison for which the temperature transition results in significant changes in radial profile. The changes suggest a slight increase in the width of the protein coat below the temperature transition.

The Effect of NaCl

Fig. 9 contains comparisons of radial density profiles in the presence and absence of NaCl for virus in (*a*) solution at temperatures above the transition temperature and (*b*) below the transition temperature, and in fibers prepared (*c*) above and (*d*) below the transition temperature. In warm solutions, the presence of 300 mM NaCl has little effect on the structure. In cold solutions significant changes in the widths and heights of the density peaks appear to occur. These may be indicative of small local changes in the configurations of the alpha helices in the virions. In fibers the concentration of NaCl may be as high as 3 M, ten times the concentration in the solutions. In warm fibers the presence of NaCl appears to have a major impact on the structure. The radius of the outer helix has decreased, the inner helix broadened, and NaCl appears to have entered the virus interior. In cold fibers, the effect of NaCl appears to be smaller but in the same direction as at higher temperatures. NaCl has almost certainly entered the virion interior in these specimens. These changes are statistically significant as judged by the *R*-factors listed in Table III.

DISCUSSION

Detection of Small Structural Changes

In assessing the work reported here, the most important point to be discussed is the reliability with which small structural changes can be characterized. Several issues need to be addressed in this regard. These include the identification and estimation of experimental errors, the validity of the models used, the number of independent measurements that have been made, and the meaning of the *R*-factor Table III.

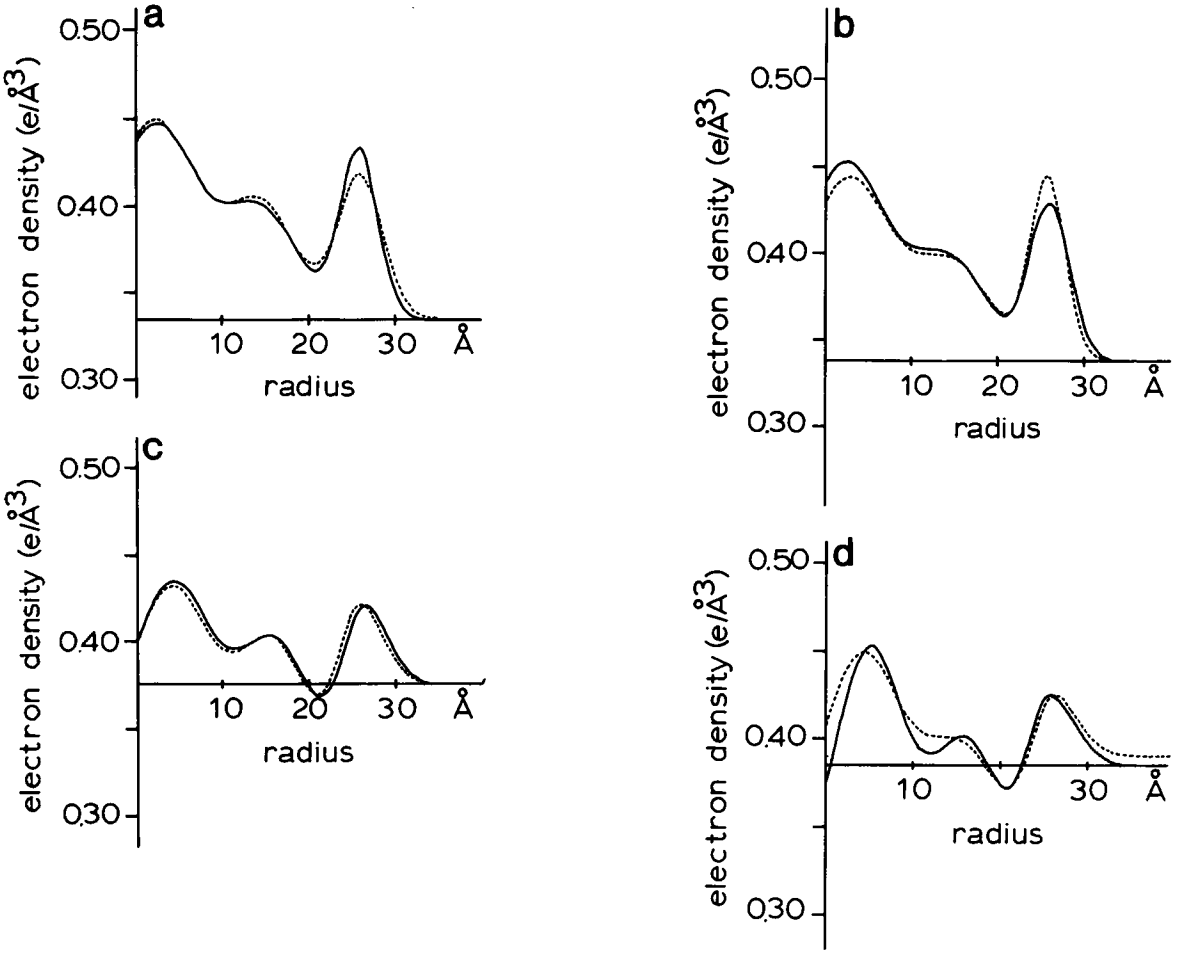

FIGURE 8 Comparison of radial density profiles for virions in specimens prepared above and below the temperature transition. Comparisons shown include specimens in (*a*) solution, (*b*) solution with 300 mM NaCl added, (*c*) fibers, and (*d*) fibers to which NaCl has been added. Solid lines represent specimens prepared at temperatures above 8°C and broken lines specimens below 8°C. The differences seen in the absence of NaCl; *a* and *c* are not significant as judged by the *R*-factor Table III.

Several kinds of experimental errors need to be considered. Errors in the specimen-to-film distance of ~1.5% could account for the radial variations seen in the electron density profiles of the fibers. In a typical experiment, this would amount to an error in measurement of ~1.2 mm. Comparisons of diffraction patterns from identical specimens taken on different cameras indicate that errors in specimens-to-film distance are <0.5 mm. Nevertheless, this may contribute to the apparent variability of virion structure in fibers. Since most errors are likely to be larger for diffraction from solutions than from fibers, the relative consistency of results from solutions indicates that some intrinsic variation of structure in fibers probably exists. In diffraction from solutions, small errors in background subtraction may account for the barely discernable differences in relative peak heights that can be seen, for instance, in the comparison of diffraction from solutions above and below the temperature transition in Fig. 5 *a*. But these differences do not result in significantly different models as judged by *R*-factor ratios in Table III. Errors in background subtraction will be significantly less for the Bragg reflections in diffraction patterns from fibers.

The question of the validity of the models used has significance mainly for the comparison of solutions and fibers. For comparison of specimens with identical average electron densities, any differences in model parameters are likely to reflect real structural differences. For comparsion of specimens with different average electron densities, the effect of solvent penetration may be significant. Could the apparent differences in the radial structure of virions in fibers and solution (Fig. 7) be due to incorrect treatment of solvent penetration? This is unlikely since the apparent radial movement is a bulk movement of all features, seen for both layers of alpha helices and, as indicated from the data in Table II, the difference in the radii of both of these layers is observed in almost all cases. Furthermore, the treatment of solvent penetration would, if anything, be expected to artifactually lower the apparent radii of structural features in fibers, whereas the reverse is observed. The seven-and nine-parameter models produced fits to the

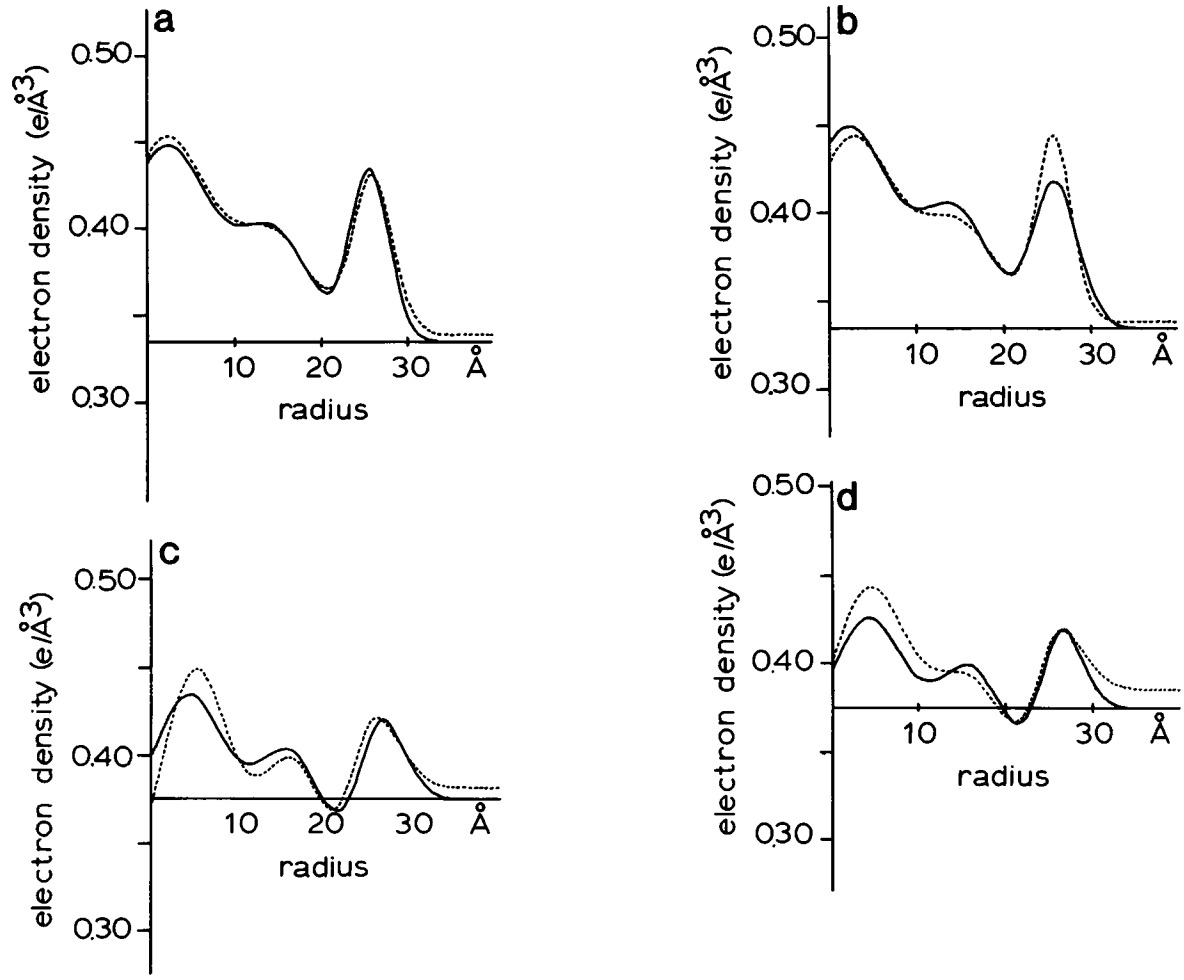

FIGURE 9 Comparison of radial density profiles for virions in specimens before and after addition of NaCl. Comparisons are shown for specimens in solution (*a*) above and (*b*) below the transition temperature and for fibers prepared (*c*) above and (*d*) below the transition temperature. Solid lines represent specimens in the absence of NaCl, broken lines represent specimens to which NaCl has been added.

data that were qualitatively the same. The decision to use models taking into account the different average electron densities was made because of the similarities among all electron density profiles constructed in this manner. Electron density profiles constructed directly from the nine-parameter models exhibited inconsistencies that appeared to be a function of the form of the model rather than of the different structures.

To make the statistical discriminations intrinsic to Table III it is necessary to know accurately the number of independent intensity measurements being used in the model refinement. In diffraction from a three-dimensional crystal this is equal to the number of unique Bragg reflections. In the case of equatorial diffraction from fibers or solutions, the number is smaller than the number of data because the measurements are oversampling the cylindrically symmetric transform, $G_{0,0}(r)$. Measurements that are closer together than the inverse of twice the diameter of the particle are in a real sense measurements of the same quantities. This oversampling leads to better estimation of the intensity but not to more independent intensities. The actual number of independent measurements is slightly larger that the product of the interval of reciprocal space sampled (in $Å^{-1}$) with twice the diameter of the virion (Makowski, L., unpublished results). The number is slightly larger than this product because continuous sampling of a transform provides relatively strong constraints on the value of the transform just outside the range of measurements. The number of independent intensity measurements for the specimens used was estimated to vary between 11 and 14 for different diffraction patterns, and these numbers were used for the statistical analysis indicated in Table III.

The statistical analysis using the *R*-factor Table III is not a completely rigorous method for distinguishing whether the structure of the virions in two different specimens is the same or not. The distinction being made with these *R*-factor ratios is whether or not the best model for data set *N* is a significantly better model for data set *N* than the best model found for data set *M*. The models reflect the corresponding structures with varying levels of accuracy. For instance, the model for specimen 3 has an

R-factor of 0.086 against data from specimen 3. Its *R*-factor against all other data sets is substantially higher. However, because of the much higher *R*-factors for models 2 and 12 against their data sets, model 3 cannot be rigorously ruled out as a model for either of these specimens. A more direct method for distinguishing among different data sets would be a direct comparison. For the case of comparisons of data from fibers and solutions this would involve interpolation onto a minimally sampled grid (e.g., Makowski, 1982) and estimates of uncertainties in these values. The problem with this method is that it could not distinguish between the effect of an actual structural change and a change in the average electron density of the specimen. This would not have provided the information required for the comparison of fibers and solutions. Consequently, the method chosen here was the comparison of least-squares sense best models. This appears to have resulted in a set of consistent conclusions based on observed differences in data, statistically significant *R*-factor differences among models, and interpretable differences in radial density profiles. In some cases radial motions of structural elements of <1 Å appear to be significant based on these criteria.

The Nature of Fibers

A rigorous comparison of the helical symmetry and equatorial transforms of filamentous bacteriophage Pf1 indicates that the structure of the virions in the fibers is very similar to that in solution. The helical symmetry of the virus does not appear to change on formation of the fiber and any gross radial motions of the structural components of the protein coat appear to be <1 Å. There does, however, appear to be some differences between the virions in fibers and in solution. In fibers there appears to be a small degree of variability in the virion structure that cannot be totally accounted for by experimental error. The data indicate that in most fibers the coat protein has an apparent radius ~0.6 Å more than in solution, but data from a few fibers do not indicate that a radial expansion has occurred. The packing of virions in fibers can be quite tight. Although the outside radius of the virion in solution is ~33 Å, lattice constants of <60 Å are frequently observed. The lattice constants of specimens studied here varied from 60 to 65 Å. Tight packing of virions may lead to structural distortions. One might expect this to result in an apparent decrease in radius as opposed to the observation of an apparent increase. However, a hexagonal distortion would result in the introduction of sixfold symmetric components of diffraction to the Bragg reflections and this could alter in an unpredictable fashion the parameters of models constructed assuming cylindrical symmetry. The apparent radial movements may be indicative of some distortion caused by packing of virions within the fibers, but the nature of that distortion cannot be unambiguously defined from the data. There is other evidence for distortions in data from Pf1 fibers. Some diffraction patterns exhibit evidence of a doubling of the axial repeat distance from 75 to 150 Å by the presence of half-order layer lines that are very weak at low angles but which, beyond 5 Å spacing, can be as intense as the integer order layer lines (Makowski, 1984). Analysis of the intensities on these layer lines indicates that the repeating unit in these virions must include at least six coat proteins.

The concentration of buffer molecules in the fibers may be over 100 times as high as in the initial solutions from which they are derived. Solvent concentration in the fiber can be calculated from lattice volumes and initial concentrations and from the nine-parameter models. These methods both result in an estimate of Tris concentration of ~0.8 M, but neither method is particularly accurate. The presence of high concentrations of buffer molecules may have some effect on the virion structure. The fibers are 30–40% solvent by weight, but how much of this could be considered bulk solvent is not known. Finely ground NaCl, when put on the surface of a fiber, is absorbed into the fiber in a matter of hours, indicating the presence of water capable of solvating NaCl. Some structural effects on the DNA, presumably due to changes in the concentration of solvent molecules, are discussed in the next section.

We can conclude that the formation of fibers of Pf1 has small but observable effects on the virion structure. The nature of these effects suggest that they are mediated through packing interactions among neighboring virus particles, and by increases in the concentrations of some solvent components.

Structure of Viral DNA

The structure of viral DNA has only been partially characterized. The number of nucleotides and the length of the virus indicates that the single-stranded DNA is highly extended, with phosphates separated axially by 5.4 Å or more. Solid state NMR (Cross et al., 1983) indicated that the O-P-O plane of the non-esterified oxygens was approximately perpendicular to the virion axis. This is consistent with the extended form of the nucleotides expected. Geometric considerations indicate that if the DNA has a helical symmetry with a 15-Å pitch (as does the protein coat) then the phosphates must be at very low radius, perhaps not more than 2.5 Å from the virion axis (Day et al., 1979). However, there are no data indicating the pitch of the viral DNA. The results obtained here suggest that the DNA conformation may be different in virions in fibers and in solutions.

The most likely place for high concentrations of buffer molecules to have an important effect on the virus structure is in the virion interior. Although this is the region of the structure least well defined by the equatorial data, statistically significant changes appear to take place there during formation of fibers. Measurement of total electrons in excess of solvent indicate that some components of the solvent enter the virion interior during fiber formation. The absolute value of these numbers is subject to some error,

but differences in them are consistent and reproducible. In solution, the number of electrons in excess of solvent is about 30 electrons per nucleotide greater than expected for the nucleotide alone. This may indicate the presence of counterions or COOH-terminal residues in the region defined by the central peak. In fibers this number increases by an average of about seven electrons per nucleotide. For comparison, 1 Na^+ ion would account for about 10 electrons, and 1 Tris molecule for about 14 electrons in excess of solvent. The formation of fibers apparently results in the penetration of the virion interior by some solvent molecules that may interact with the DNA in less than stoichiometric quantities.

The radius of the central peak changes significantly between solution and fibers. The radial change is consistent and reproducible. It is not solely a reflection of solvent penetration since the amount of electron-dense solvent constituents entering the virion interior is small compared with the total represented by this peak. This movement apparently represents a change in DNA conformation or radius. A change in the radius of the DNA is presumably driven by changes in DNA–DNA or DNA–protein interactions that, in turn, must be modulated by the presence of small amounts of solvent components in the virion interior. This responsiveness of DNA conformation to solvent changes suggests that any geometric constraints on its conformation may not be as strict as suggested by the symmetry considerations discussed by Day et al. (1979).

The Temperature Transition

The change in helical symmetry that occurs in the Pf1 virion at ~8°C appears to be very similar when studied by diffraction from fibers or from solutions. Any changes in the radial structure are too small to be characterized by the techniques used here. In fibers, statistically significant changes occur in the presence of NaCl, but the small variability of virion structure in fibers makes these changes difficult to interpret. It seems clear that, at the very least, some change in the structure of the NH_2-terminal alpha helices is indicated by the bulk of the available data. Comparison of the 7-Å resolution three-dimensional electron density maps of Pf1 above and below the transition temperature (Makowski, 1984) indicated that the COOH-terminal alpha helices do not move during the temperature transition but that at low temperature, the alpha helices in the outer layer are ~4° closer to axial in orientation than they are at high temperatures.

The physical and chemical data available make possible a discussion of the possible origin of this structural transition. Measurement of the relative apparent isopotential specific volumes (Hinz et al., 1980) of Pf1 and fd (which does not exhibit a comparable temperature transition) shows that, relative to fd, Pf1 increases in specific volume by ~65 $Å^3$ per coat protein (about the volume of two water molecules). The calorimetrically determined transition enthalpy corresponds to ~3.46 kcal/mol per coat protein. Both of these measurements are consistent with the transition involving a decrease in the contact of hydrophobic side chains with water as temperature increases. The change in enthalpy for moving one molecule of methane from water into benzene is ~2.8 kcal/mol (Frank and Evans, 1945; Kauzmann, 1959). The volume change associated with this transfer is 37.7 $Å^3$, mainly because water molecules ordered around a methane molecule occupy less volume than they do in bulk water. Thus, during the increase in temperature across the Pf1 structural transition, the enthalpy change observed corresponds to that of the movement of ~1.2 methane molecules from water into benzene. The observed volume change (relative to fd) corresponds to the movement of 1.7 methane molecules from water into benzene. During the transition it is possible that one or more hydrophobic side chains change position to lower the amount of their surface in contact with water. This driving force may be responsible for the change in helical symmetry and the slight change in radial and azimuthal tilt observed in the NH_2-terminal alpha helices.

The Effect of NaCl

The presence of NaCl appears to have a significant effect on the structure of Pf1. It results in a small decrease in the axial repeat distance of viruses in fibers and may cause a small narrowing of the protein coat. It penetrates the virus interior where it may affect the configuration of the viral DNA. And its presence appears to amplify the effects of the temperature transition. The effect of NaCl on Pf1 virion structure was first recognized by Raman spectroscopy (Thomas et al., 1983). That study concluded that NaCl narrows the range of alpha helical conformations in the virus and that Na^+ ions may interact with the main chain carbonyl groups in the protein coat. No evidence for any change in the proportion of alpha helical conformation was detected. The available data leave open a great many possibilities for the mode of action of the NaCl. The slight compaction of the structure in solvent with increased ionic strength might occur to minimize interactions between hydrophobic groups and solvent. Or the compaction could be caused by the postulated interaction of Na^+ ions with carbonyls. The compaction might lead to a more rigid virion that would undergo more exaggerated movements during the temperature transition.

Structural Responsiveness and Flexibility

The Pf1 virion exhibits more responsiveness to changes in environment than do rigid rod viruses such as tobacco mosaic virus. This may be a requirement for the survival of the virion which is almost 2-μm long and only 60 Å in diameter. The Pf1 virion, although quite flexible, as judged by electron micrographs in which the virus particles exhibit substantial curvature, is still quite sensitive to shear (Marvin and Hohn, 1969). If Pf1 were a rigid rod it would be much more sensitive to shear and this would be a strong selective disadvantage for the virus. Curvature of the virion

is a response to torque. For flexibility, the outer layer of helices needs to be more responsive than the inner since any rigidity in the outer layer would resist curvature with a longer moment arm than any structural rigidity in the inner layers. Detailed analysis of the structural changes observed here suggests that, in general, more changes appear to be associated with the outer layer of helices than the inner.

Structural responses to environmental stress may involve motions of individual sidechains or concerted motions of secondary structural elements in which, for instance, alpha helices may move as a relatively rigid unit. The experiments described here can detect only concerted motions. There is evidence that small movements of the alpha helices occur in response to the formation of fibers, temperature changes, and changes in NaCl concentration. In a crystallographic study of lysozyme at 1 and 1,000 atm pressure (Kundrot and Richards, 1986) it was found that pressurization resulted in a compression of the molecule. To a first approximation, secondary structures such as alpha helices moved as rigid bodies in response to the pressure change. Small movements of secondary structures may represent a common response of proteins to environmental stress.

The importance of hydrophobic interactions for the stabilization of the virion may also contribute to its structural flexibility. There are three sets of intersubunit bonds possible in the Pf1 surface lattice: along the 5-start helices, the 6-start helices, and the 11-start helices. If polar interactions occurred along all three directions, then it is likely that the phage particles would be rigid. Consider, for instance, a parallelogram constructed of four pieces of wood connected by hinges at the vertices. This structure is mechanically very flexible. Join one pair of opposite vertices with a diagonal rod and a rigid structure is formed. Analysis of potential interactions among the subunits indicated (Makowski, 1984) that polar interactions among subunits were unlikely along the 5-start directions. The lack of polar interactions along the 5-start direction in Pf1 may be crucial for the flexibility of the phage particles. This pattern of interactions is also likely to be partially responsible for the responsiveness of the Pf1 virion to other environmental changes. This responsiveness may be only a side effect of a strategy for defense against shear. Or it may be a more general strategy for defense against a variety of environmental stresses. The responsiveness of the virion allows it to maintain viability in the absence of a rigid shell about the viral genome.

We thank Drs. Keith Moffat and Walter Phillips for help with experiments performed at CHESS and Brandeis University.

This work was supported by National Institutes of Health Grant GM-29829 to L. Makowski.

Received for publication 14 November 1986 and in final form 13 April 1987.

REFERENCES

Chothia, C. H. 1975. Structural invariants in protein folding. *Nature (Lond.).* 254:304–308.

Cross, T. A., P. Tsang, and S. J. Opella. 1983. Comparison of protein and deoxyribonucleic acid backbone structures in fd and Pf1 bacteriophages. *Biochemistry.* 22:721–726.

Day, L. A., R. L. Wiseman, and C. J. Marzec. 1979. Structural models for DNA in filamentous viruses with phosphates near the center. *Nucl. Acids Res.* 7:1393–1403.

Earnshaw, W., S. Casjens, and S. C. Harrison. 1976. Assembly of the head of bacteriophage P22: x-ray diffraction from heads, proheads and related structures. *J. Mol. Biol.* 104:387–410.

Frank, H. A., and M. W. Evans. 1945. Free volume and entropy in condensed systems. III. Entropy in binary liquid mixtures; partial molal entropy in dilute solutions; structure and thermodynamics in aqueous electrolytes. *J. Chem. Phys.* 13:507–513.

Glucksman, M., D. Hay, and L. Makowski. 1986. X-ray diffraction from magnetically oriented solutions of macromolecular assemblies. *Science (Wash. DC).* 231:1273–1276.

Hamilton, W. C. 1965. Significant tests on the crystallographic R-factor. *Acta Crystallogr.* 18:502–510.

Hinz, H. J., K. O. Greulich, H. Ludwig, and D. A. Marvin. 1980. Calorimetric, density and circular dichroism studies of the reversible structural transition on Pf1 filamentous virus. *J. Mol. Biol.* 144:281–289.

Kauzmann, W. 1959. Some factors in the interpretation of protein denaturation. *Adv. Protein Chem.* 14:1–63.

Klug, A., F. H. C. Crick, and H. W. Wyckoff. 1958. Diffraction by helical structures. *Acta Crystallogr.* 11:199–213.

Kundrot, C. E., and F. M. Richards. 1986. The crystallographic structure of lysozyme at 1000 atmospheres. *Biophys. J.* 49(2, Pt. 2):288a. (Abstr.)

Makowski, L. 1982. The use of continuous diffraction data as a phase constraint. II. Application to fiber diffraction data. *J. Appl. Cryst.* 15:546–557.

Makowski, L. 1984. Structural diversity in filamentous bacteriophages. *In* Biological Macromolecules and Assemblies, Vol. I. The Viruses. A. McPherson, editor. John Wiley & Sons, Inc., New York. 203–253.

Makowski, L., and D. L. D. Caspar. 1978. Filamentous bacteriophage Pf1 has 27 subunits in its axial repeat. *In* The Single-stranded DNA Phages. D. T. Denhardt, D. Dressler, and D. S. Ray, editors. Cold Spring Harbor Laboratory, Cold Spring Harbor, NY. 627–643.

Makowski, L., D. L. D. Caspar, and D. A. Marvin. 1980. Filamentous bacteriophage Pf1 structure determined to 7 A resolution by refinement of models for the alpha helical subunit. *J. Mol. Biol.* 140:149–181.

Marvin, D. A., and B. Hohn. 1969. Filamentous bacterial viruses. *Bacteriol. Rev.* 33:172–209.

Marvin, D. A., and E. J. Wachtel. 1975. Structure and assembly of filamentous bacterial viruses. *Nature (Lond.).* 253:19–23.

Marvin, D. A., and E. J. Wachtel. 1976. Structure and assembly of filamentous bacterial viruses. *Philos. Trans. R. Soc. Lond. B Biol. Sci.* 276:81–98.

Marvin, D. A., C. Nave, J. E. Ladner, A. G. Fowler, R. S. Brown, and E. J. Wachtel. 1981. Macromolecular structural transitions in Pf1 filamentous bacterial viruses. *In* Structural Aspects of Recognition and Assembly in Biological Macromolecules. M. Balaban, J. L. Sussman, W. Traub, and A. Yonath, editors. Balaban ISS, Rehovot. 891–910.

Moody, M., and L. Makowski. 1981. The structure of the tail core of bacteriophage T2. *J. Mol. Biol.* 150:217–245.

Nave, C., A. G. Fowler, S. Malsey, D. A. Marvin, H. Siegrist, and E. J. Wachtel. 1979. Macromolecular structural transitions in Pf1 filamentous bacterial virus. *Nature (Lond.).* 281:232–234.

Nave, C., R. S. Brown, A. G. Fowler, J. E. Ladner, D. A. Marvin, S. W. Provencer, A. Tsugita, J. Armstrong, and R. N. Perham. 1981. Pf1 filamentous bacterial virus. X-ray fibre diffraction analysis of two heavy atom derivatives. *J. Mol. Biol.* 149:675–707.

Sasaki, S., and S. Fujime. 1987. Dynamic light-scattering study on changes in flexibility of filamentous bacteriophage Pf1 with temperature. *Biophys. J.* In press.

Stubbs, G., and L. Makowski. 1982. Coordinated use of isomorphous replacement and layer-line splitting in the phasing of fiber diffraction patterns. *Acta Cryst.* A38:417–425.

Thomas, G. J., B. Prescott, and L. A. Day. 1983. Structural similarity, difference and variability in the filamentous viruses fd, If1, IKe, Pf1 and Xf. Investigation by laser Raman spectroscopy. *J. Mol. Biol.* 165:321–356.

Torbet, J., and G. Maret. 1979. Fibers of highly oriented Pf1 bacteriophage produced in a strong magnetic field. *J. Mol. Biol.* 134:843–845.

Torbet, J., and G. Maret. 1981. High-field magnetic birefringence study of the structure of rodlike phages Pf1 and fd in solution. *Biopolymers.* 20:2657–2669.

Wachtel, E. J., F. J. Marvin, and D. A. Marvin. 1976. Structural transition in a filamentous protein. *J. Mol. Biol.* 107:379–383.